

University of Nebraska - Lincoln

DigitalCommons@University of Nebraska - Lincoln

Marjorie A. Langell Publications

Published Research - Department of Chemistry

December 2005

Cu₂O(1 1 0) formation on Co₃O₄(1 1 0) induced by copper impurity segregation

S. C. Petitto

University of Nebraska - Lincoln

Marjorie Langell

University of Nebraska - Lincoln, mlangell1@unl.edu

Follow this and additional works at: <https://digitalcommons.unl.edu/chemistrylangell>

 Part of the [Chemistry Commons](#)

Petitto, S. C. and Langell, Marjorie , "Cu₂O(1 1 0) formation on Co₃O₄(1 1 0) induced by copper impurity segregation" (2005). *Marjorie A. Langell Publications*. 13.

<https://digitalcommons.unl.edu/chemistrylangell/13>

This Article is brought to you for free and open access by the Published Research - Department of Chemistry at DigitalCommons@University of Nebraska - Lincoln. It has been accepted for inclusion in Marjorie A. Langell Publications by an authorized administrator of DigitalCommons@University of Nebraska - Lincoln.

Cu₂O(1 1 0) formation on Co₃O₄(1 1 0) induced by copper impurity segregation

S. C. Petitto and M. A. Langell*

Department of Chemistry, University of Nebraska–Lincoln, Lincoln, NE 68588-0304

**Corresponding author. Email: mlangell@unl.edu*

Abstract: The surface crystal structure of the Co₃O₄(1 1 0) spinel was characterized by low energy electron diffraction (LEED), X-ray photoelectron spectroscopy (XPS), and Auger electron spectroscopy (AES). Well-defined LEED diffraction patterns showed an unreconstructed Co₃O₄(1 1 0) surface in Type A termination, and XPS and Auger indicated the surface to be stoichiometric with octahedral and tetrahedral cation sites occupied by 3+ and 2+ cations, respectively. The experimental lattice parameters of 8.22 Å ± 0.2 Å and 5.50 Å ± 0.2 Å in the (0 0 1) and (1 1 0) directions, respectively, are in agreement with a bulk-terminated unit cell.

The impurities: K, Ca, Na, and Cu segregated to the surface after prolonged heating to 630 K. K, Ca and Na could easily be removed by routine cleaning procedures and did not affect the Co₃O₄(1 1 0) structure or stoichiometry detectably in the submonolayer levels at which they were observed. However, the copper impurity resulted in the formation of a Cu₂O(1 1 0) overlayer, with the accompanying reduction of the spinel surface to a rocksalt metal monoxide-like surface. The copper oxide formed a distorted hexagonal overlayer incommensurate with that of the Co₃O₄(1 1 0) stoichiometric surface and with periodic spacings of 3.86 Å ± 0.2 Å in the (0 0 1) and 4.10 Å ± 0.2 Å in the (1 1 0) directions in agreement with Cu₂O(1 1 0) bulk termination. The Co₃O₄(1 1 0) substrate could not be fully re-oxidized until all detectable copper had been removed from the surface.

Keywords: Low energy electron diffraction (LEED), Surface segregation, Cobalt oxides, Copper oxides

1. Introduction

An in-depth understanding of the physical and chemical surface properties of transition metal oxides is

necessary for the continued development of these heterogeneous materials and their technological applications. The cobalt oxide spinel, Co₃O₄, is used in a variety of catalytic processes including: partial oxida-

tion [1–3], fuel-efficient engines [4, 5], coatings in fuel cells [6], decomposition of hydrogen peroxide [2, 7] and oxidation of carbon monoxide [4, 8, 9, & 10]. Catalyst performance also can be improved by doping or alloying with other metals and several mixed-metal cobalt oxide spinels, including $\text{Cu}_x\text{Co}_{3-x}\text{O}_4$ [1, 3, 7, 11–17], $\text{Cr}_x\text{Co}_{3-x}\text{O}_4$ [15], $\text{Li}_x\text{Co}_{3-x}\text{O}_4$ [17], $\text{Mn}_x\text{Co}_{3-x}\text{O}_4$ [16, 18], and $\text{Ni}_x\text{Co}_{3-x}\text{O}_4$ [16, 17, & 19] have been proposed to enhance specific chemical or physical properties of the cobalt oxide spinel.

Co_3O_4 single crystals naturally form with a truncated octahedron morphology comprised of (1 1 0) and (1 1 1) crystal faces [20, 21]. The cubic spinel lattice unit cell contains 56 atoms and has a lattice constant of 8.084 Å along the (0 0 1) direction and 5.713 Å along the $(\bar{1} 1 0)$ direction [13, 22, & 23]. In the spinel lattice structure, half the octahedral sites of the unit cell are occupied by sixteen M^{3+} cations and one-eighth of the tetrahedral sites are occupied by eight M^{2+} cations, with the octahedral and tetrahedral sites formed by 32 O^{2-} anions packed in a face-centered cubic (FCC) lattice [13, 22]. Co_3O_4 is antiferromagnetic in which each Co^{2+} cation is surrounded by four nearest neighbors with opposite spin [23] and it is a p-type semiconductor with a band gap of about 2.2 eV [24].

Dopants or impurities can have a substantial effect on electronic and magnetic properties [10], [25] and [26] and they can affect the stability of the spinel structure [12, 27]. Transition metals that substitute for the cobalt in the $\text{M}^{2+}\text{M}_2^{3+}\text{O}_4$ spinel (M^{2+} , M^{3+} = cobalt or dopant metal) have been observed to change the distribution of cation oxidation states, creating an inverted or partially inverted spinel structure in which the M^{3+} cations now occupy both octahedral and tetrahedral sites and at least some of the M^{2+} are found in octahedral sites [12, 15–17]. The dopants also can cause phase separation accompanied by the formation of a totally different crystal structure [16, 27, & 28]. Since impurities tend to segregate to the substrate surface, even low bulk concentrations can be substantial at the surface and therefore can have a profound effect on the structure and chemistry of the material; such impurity segregation effects have been ob-

served in doped Co_3O_4 samples [3, 7, 11, 25, & 29]. Addition of copper to the cobalt spinel, for example, can be accommodated without a change in crystal structure for concentrations of up to $x \leq 0.9$ [12, 14, & 15], after which phase separation is observed to form $\text{Cu}_{1-x}\text{Co}_{2+x}\text{O}_4$ and CuO [14, 27, & 28]. The $\text{Cu}_{1-x}\text{Co}_{2+x}\text{O}_4$ spinels are partially inverted, with Cu^{2+} occupying both octahedral and tetrahedral sites and displacing some of the Co^{3+} into tetrahedral sites.

Few single crystal surface studies have been performed on the spinel Co_3O_4 [30, 31] and none have been reported for doped Co_3O_4 single crystals. However, Co_3O_4 thin crystalline films have been grown epitaxially on $\text{CoO}(1 0 0)$ [32–34] and polycrystalline photoemission data can readily be found [35–38]. X-ray photoelectron spectroscopy (XPS) has been previously used to investigate the surface chemical composition and chemical environment of the Co_3O_4 surface, the latter of which can be determined from satellite structure and spectral peak shape [18, 30, 32–37, 39, & 40]. The stoichiometric Co_3O_4 XPS spectrum yields relatively sharp cobalt $2p_{3/2}$ and $2p_{1/2}$ features with weak, broadened satellite structure and the spectra are consistent with low-spin, diamagnetic octahedral Co^{3+} cations and tetrahedral Co^{2+} cations within the FCC O^{2-} sublattice [32–34, 38, 41, & 42]. In contrast, broad cobalt 2p peaks with intense satellite structure are observed for CoO , in which the octahedrally coordinated Co^{2+} is high-spin $3d^7$, showing strong electron correlation and measurable hybridization with the O 2p band to produce intense final state effects in the photoemission spectrum [38, 39, 42–44].

In this paper, $\text{Co}_3\text{O}_4(1 1 0)$ single crystals of both the stoichiometric and Cu impurity-segregated surfaces were investigated with LEED, AES, and XPS and the identity of the copper-segregated selvedge was ascertained. The stoichiometric cobalt 2p XPS spectrum was representative of a spinel surface with weak satellite features located about 9 eV higher in binding energy than the $2p_{3/2,1/2}$ peaks. LEED patterns for the Co_3O_4 stoichiometric surface were representative of an unreconstructed cubic (1 1 0) surface [18] and [45] with symmetry-equivalent sets

of diffractions features identified by their intensity variation with primary electron beam energy. Upon substrate annealing calcium, potassium, sodium, and copper impurities segregated to the substrate surface. All but copper were easily removed and were found at submonolayer levels. The presence of copper resulted in a poorly ordered Cu₂O(1 1 0) overlayer with a maximum thickness of about six layers. As a result of the copper oxide overlayer formation, the underlying Co₃O₄ substrate was reduced to CoO-like composition. The spinel surface could not be fully re-oxidized to Co₃O₄ even with prolonged annealing under oxygen, and remained reduced as long as copper was present.

2. Experimental

The Co₃O₄ single crystal was wrapped with gold foil (Alfa Aesar, 0.025 mm, 99.95%) so that the 3 mm × 3 mm (1 1 0) sample face was completely exposed for analysis.¹ The sample was then suspended between the sample mount posts by the two-tantalum heating wires (0.25 mm diameter, Alfa Aesar, 99.9%) and the temperature was measured using a chromel–alumel thermocouple spot welded to the gold foil at the back of the sample. The manipulator had provisions for resistive heating and conductive cooling through Ta wires with cooling accomplished through an open-cycle liquid-nitrogen cryostat. The Co₃O₄ crystal could be easily cooled to 100 K and heated to 1000 K.

The working base pressure of the UHV chamber was $\sim 3 \times 10^{-8}$ Pa. The Co₃O₄(1 1 0) spinel sample surface was cleaned using cycles of Ar⁺ sputtering (2.3 μ A/cm²) for 30 min at 300 K, then O₂ (1.3×10^{-5} Pa) annealing for 20 min at 630 K, and UHV annealing for 10 min at 630 K to remove any excess surface oxygen that may have resulted from the previous O₂ anneal. This treatment has been previously shown to yield a stoichiometric surface [30]. Auger electron spectroscopy (AES) was employed to determine stoichiometry and impurity concentrations

and the surface was considered clean when contaminants were below the level of AES detection. AES spectra were acquired in the $N(E)$ vs. E mode with a Physical Electronics (Φ) 15-255G double-pass cylindrical mirror analyzer (DPCMA) at 2 kV primary electron, 1 eV resolution, and a scan rate of 5 eV/second. Data were signal averaged for 10 scans.

The surface chemical nature and stoichiometry were determined by X-ray photoelectron spectroscopy (XPS), with spectra generated with a Φ 04-548 dual X-ray anode using the MgK α photon source ($h\nu = 1253.6$ eV). The anode was controlled by a Φ 50-096 X-ray source control/supply, and the data were energy analyzed by the same the Φ 15-255G DPCMA used in AES, but in constant pass mode with a pass energy of 25 eV.

To compensate for any charging effects or change in contact potential difference between the spectrometer and the sample, all XPS data were referenced to the Co₃O₄ lattice O 1s peak set to 529.6 eV [18, 19, 31–33] and fitted with a minimum number of Gaussian–Lorentzian peaks using XPSPEAK 4.1 [46] after the removal of a Shirley background [47]. Day to day changes in the uncorrected binding energies were generally constant to within 0.2 eV. Spectrometer energy scales were calibrated electronically and periodically checked in XPS using gold foil Au 4f_{7/2} at 84.8 eV and NiO(1 0 0) Ni 2p_{3/2} at 854.8 eV for the range and NiO(1 0 0) O 1s at 529.6 eV for the absolute value. XPS binding energies are believed to be accurate to 0.1 eV. AES spectra were taken with 1 eV resolution.

LEED patterns were obtained at 300 K with a set of Vacuum Generator Microtech four grid LEED optics controlled by VG Mirocotech Model 8011 electronics. The primary beam energy ranged from 25 eV to 165 eV with 2.30–2.50 A filament current and a 1 kV screen voltage. Diffraction patterns were displayed and recorded using an EHD kam-Pro02IR CCD video camera interfaced to a monochrome video monitor and the resulting LEED intensities were analyzed with EE2000 SMARTOOL for diffraction images composites of at least 16 average scans.

¹ Kindly provided through the generosity of W.H. McCarroll, Department of Chemistry, Biochemistry, and Physics, Rider University, Lawrenceville, NJ.

3. Results

The structure and composition of the $\text{Co}_3\text{O}_4(1\ 1\ 0)$ surface have previously been described in detail [30] and the surface analysis data on the clean, stoichiometric substrate are provided here for reference to show the surface quality. The AES spectrum of the as-introduced sample is shown in Fig. 1a and reveals several common surface contaminants: K, C, and Ca in submonolayer coverage. These impurities were easily removed by Ar^+ sputtering, followed by O_2 and UHV annealing to restore surface order and stoichiometry (Fig. 1b). Once the intensities of the surface contaminants were below the AES detection limit, XPS was used to confirm the relative oxygen to cobalt surface concentrations. The calculated oxygen to cobalt ratio was $C_{\text{O}}/C_{\text{Co}} = 1.28 \pm 0.15$, in agreement to within error of the spinel stoichiometry [30, 32, 38].

LEED data for the clean, stoichiometric $\text{Co}_3\text{O}_4(1\ 1\ 0)$ surface were obtained at incident energies of 25–152 eV and a representative pattern at 98 eV is shown in Fig. 2. Two possible termination

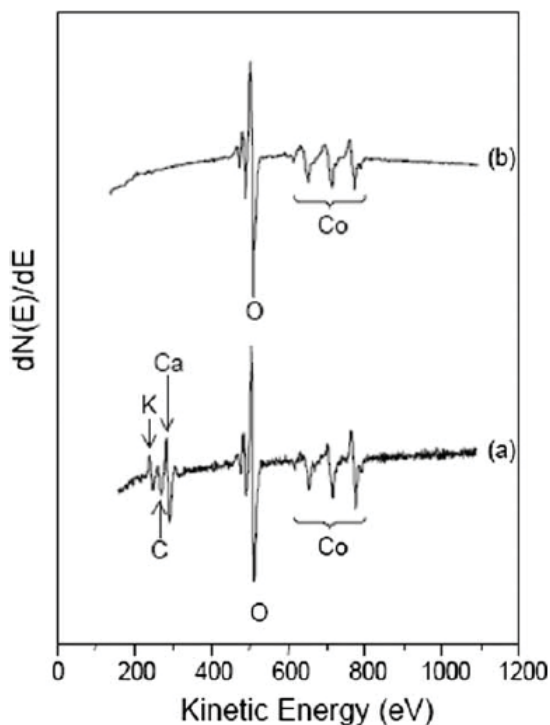


Figure 1. AES of $\text{Co}_3\text{O}_4(1\ 1\ 0)$: (a) as-introduced surface and (b) after sputtering and annealing cleaning cycles resulting in a clean, stoichiometric surface.

layers exist for the unreconstructed $(1\ 1\ 0)$ spinel surface and they are depicted schematically in Fig. 3. The $\text{Co}_3\text{O}_4(1\ 1\ 0)$ LEED shows the well-ordered rectangular reciprocal space pattern expected for the unreconstructed $(1\ 1\ 0)$ spinel surface with Type A termination [30] and [45]. As the primary beam energy is increased, the observed diffraction beams are modulated in intensity by Bragg diffraction and several sets of symmetry-related features, linked by their intensity modulation behavior, emerge from the analysis (Fig. 2). The experimentally acquired intensity vs. voltage (I - V) sets of $(1, 1)$, $(1, \bar{1})$ with $(\bar{1}, 1)$ and $(0, 2)$, $(0, \bar{2})$ with $(2, 0)$, $(\bar{2}, 0)$ features corroborate the twofold symmetric surface lattice expected for the Type A unreconstructed lattice termination. The LEED diffraction features were determined to have a periodic spacing of $8.22\ \text{\AA} \pm 0.2\ \text{\AA}$ and $5.50\ \text{\AA} \pm 0.2\ \text{\AA}$ in the $(0\ 0\ 1)$ and $(\bar{1}\ 1\ 0)$ directions, respectively, which agree within error to the bulk unit cell parameters of $8.084\ \text{\AA} \times 5.713\ \text{\AA}$ for the $\text{Co}_3\text{O}_4(1\ 1\ 0)$ plane [13]. The surface unit cell is, thus, in agreement with the bulk-terminated periodic spacing. No sample charging was observed over the incident electron energy range and all images were acquired at room temperature.

Prolonged annealing of the $\text{Co}_3\text{O}_4(1\ 1\ 0)$ surface at an elevated temperature of 630 K resulted in the segregation of bulk impurities: K, Ca, Na, and Cu (Fig. 4a). The maximum surface concentrations of the K, Ca and Na impurities were estimated to be in submonolayer coverage for even the most heavily segregated surfaces. Calcium, potassium, and sodium were easily removed with the sputtering/annealing procedure detailed in the experimental section above. However, the copper impurity remained on the surface with repeated cleaning cycles and the surface concentration continued to increase to a maximum of approximately 7 Cu to 10 Co atoms, as estimated by AES peak-to-peak intensities, after 20 h annealing (Fig. 4b).

The copper impurity-segregated surface was further investigated with XPS and LEED. The XPS data for the $\text{Co}_3\text{O}_4(1\ 1\ 0)$ -Cu surface changed substantially from that of the clean, stoichiometric $\text{Co}_3\text{O}_4(1\ 1\ 0)$ substrate (Fig. 5) and, after copper segregation, the Co 2p spectrum indicates that the

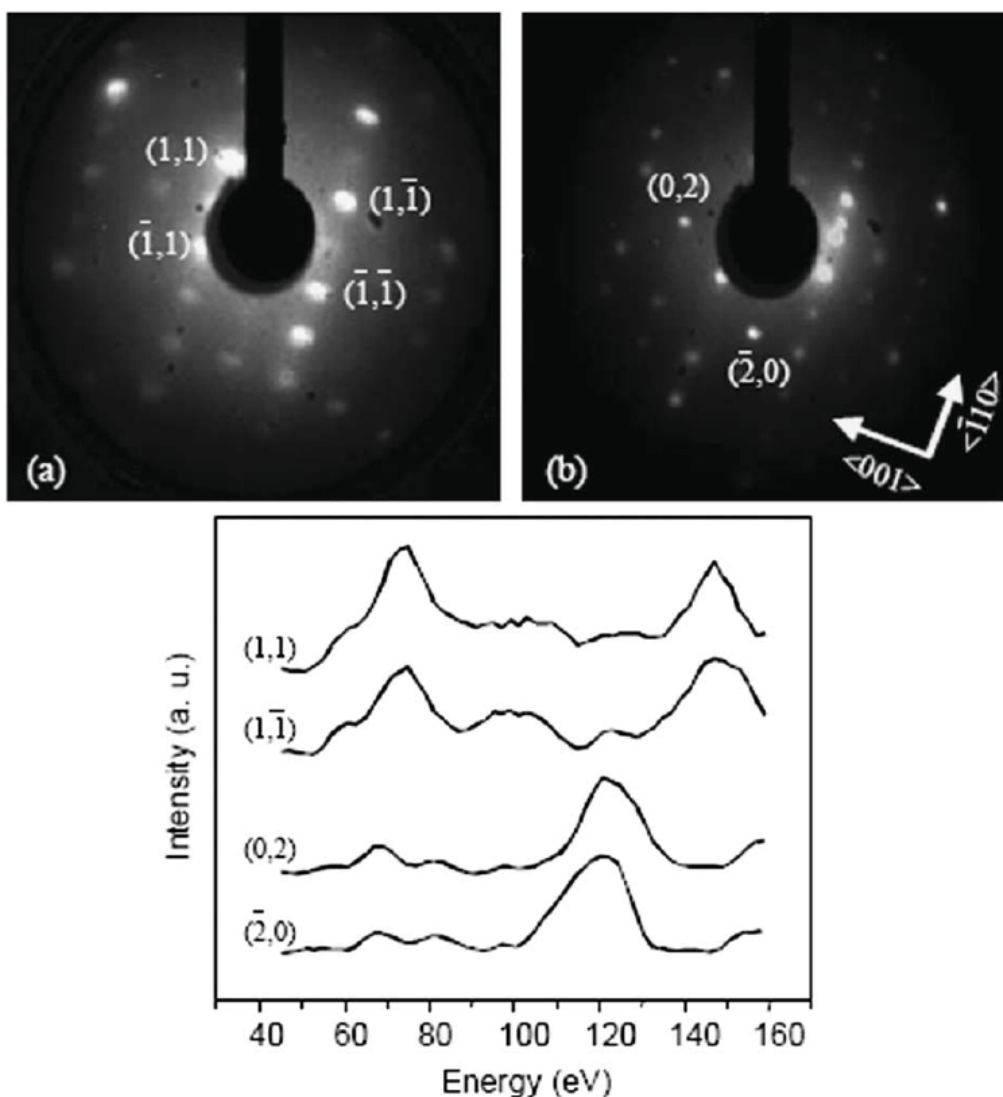


Figure 2. LEED data for the clean, stoichiometric Co₃O₄(1 1 0) surface acquired at room temperature at an incident electron beam energy of (a) 98 eV and (b) 122 eV with the corresponding measured I - V curves for the (1, 1), $(\bar{1}, 1)$, and (0, 2), $(\bar{2}, 0)$ diffraction beams. I - V data are experimentally acquired in 2 eV increments.

surface was reduced to a CoO-like composition. After correcting for sensitivity factors [30] and with the assumption of a homogeneous near-surface elemental distribution, the XPS integrated peak intensities for the copper-segregated surface gave an oxygen to cobalt concentration ratio of $C_{\text{O}}/C_{\text{Co}} = 0.94$, indicating that copper segregation is accompanied by significant surface reduction. Data presented below argue for an inhomogeneous concentration distribution in which a thin film of copper oxide largely covers a reduced cobalt oxide selvedge.

While the Co 2p satellite region of the clean, stoichiometric surface (Fig. 5a) shows only weak intensity characteristic of the Co₃O₄ spinel surface, the copper-segregated surface now clearly results in intense satellite structure representative of octahedrally coordinated Co²⁺ cations found in CoO (Fig. 5b). This satellite structure is shifted by about 3 eV to lower binding energies, 785.5 eV and 802.1 eV, closer to that found for CoO [32–39]. The main cobalt 2p_{3/2} and 2p_{1/2} photoemission binding energies also shift upon copper segregation from 779.8 eV

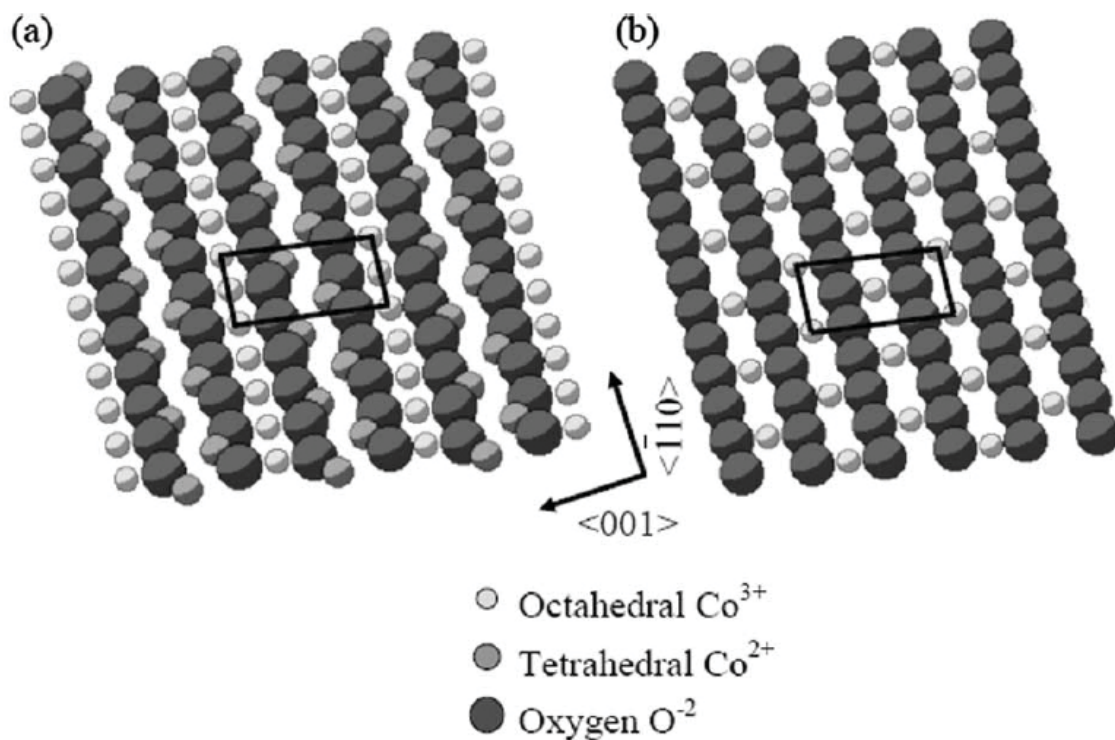


Figure 3. Bulk termination planes of $\text{Co}_3\text{O}_4(1\ 1\ 0)$: (a) Type A with Co^{3+} cations occupying octahedral sites and Co^{2+} cations in tetrahedral sites and (b) Type B with Co^{3+} cations occupying octahedral sites and vacant tetrahedral sites.

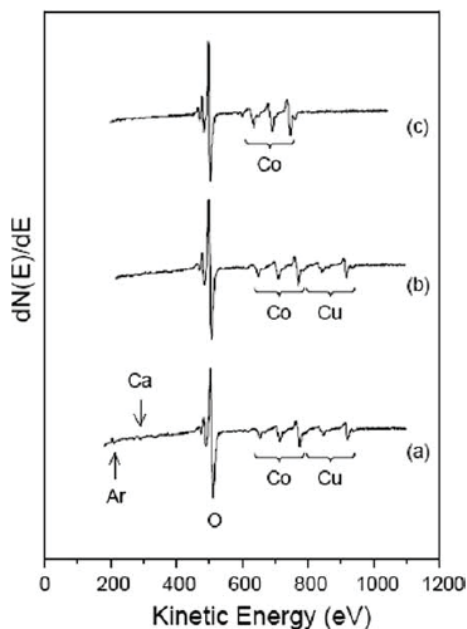


Figure 4. AES of $\text{Co}_3\text{O}_4(1\ 1\ 0)$: (a) “dirty” impurity-segregated surface, (b) after sputtering/annealing cleaning cycles resulting in a “clean” $\text{Co}_3\text{O}_4(1\ 1\ 0)$ -Cu surface, and (c) re-oxidized, stoichiometric $\text{Co}_3\text{O}_4(1\ 1\ 0)$ surface.

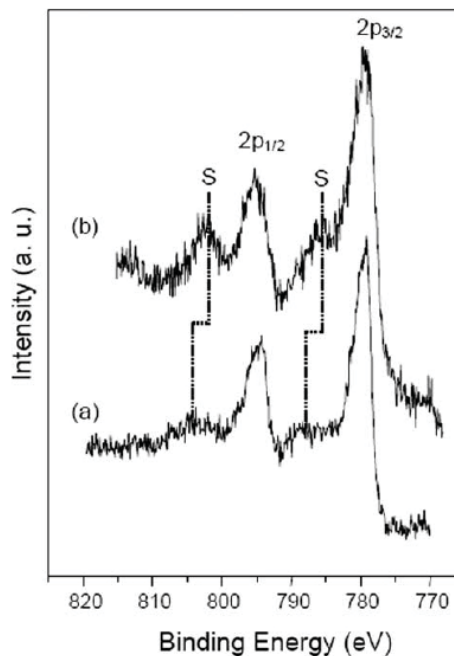


Figure 5. XPS spectra for the Co 2p region (a) stoichiometric $\text{Co}_3\text{O}_4(1\ 1\ 0)$ and (b) $\text{Co}_3\text{O}_4(1\ 1\ 0)$ -Cu acquired with $\text{MgK}\alpha$ radiation.

and 795.7 eV for the stoichiometric substrate to 779.2 eV and 795.2 eV for the copper-segregated surface, with substantial broadening to higher binding energy. The O 1s region for the Co₃O₄(1 1 0)–Cu surface remained unchanged to within the error of the measurement.

The Co₃O₄(1 1 0)–Cu surface LEED data were acquired at room temperature over an energy range of 102 eV to 150 eV and are shown in Fig. 6. The diffraction patterns are not as clearly defined as are the clean, stoichiometric Co₃O₄(1 1 0) patterns, indicative of a less well-ordered surface structure. A rectangular pattern resulting from the reduced Co₃O₄(1 1 0) surface also is weakly present, but is obscured by the copper-

segregated pattern, which forms a distorted hexagon in a periodicity that is not easily related to the lattice parameters of the Co₃O₄(1 1 0) substrate or with that expected from CoO(1 1 0). The distorted hexagonal LEED pattern was only observed when the copper impurity was present on the surface and did not appear to be affected by K, Ca or Na impurities when they were present. When the surface contaminants K, Ca, and Na were present, but no Cu, the LEED patterns resembled that of the stoichiometric Co₃O₄(1 1 0) Type A termination structure. The periodic spacing of the Cu-overlayer diffraction features along the (0 0 1) direction corresponds to $3.86 \text{ \AA} \pm 0.2 \text{ \AA}$ and along the (1 1 0) direction to $4.10 \text{ \AA} \pm 0.2 \text{ \AA}$.

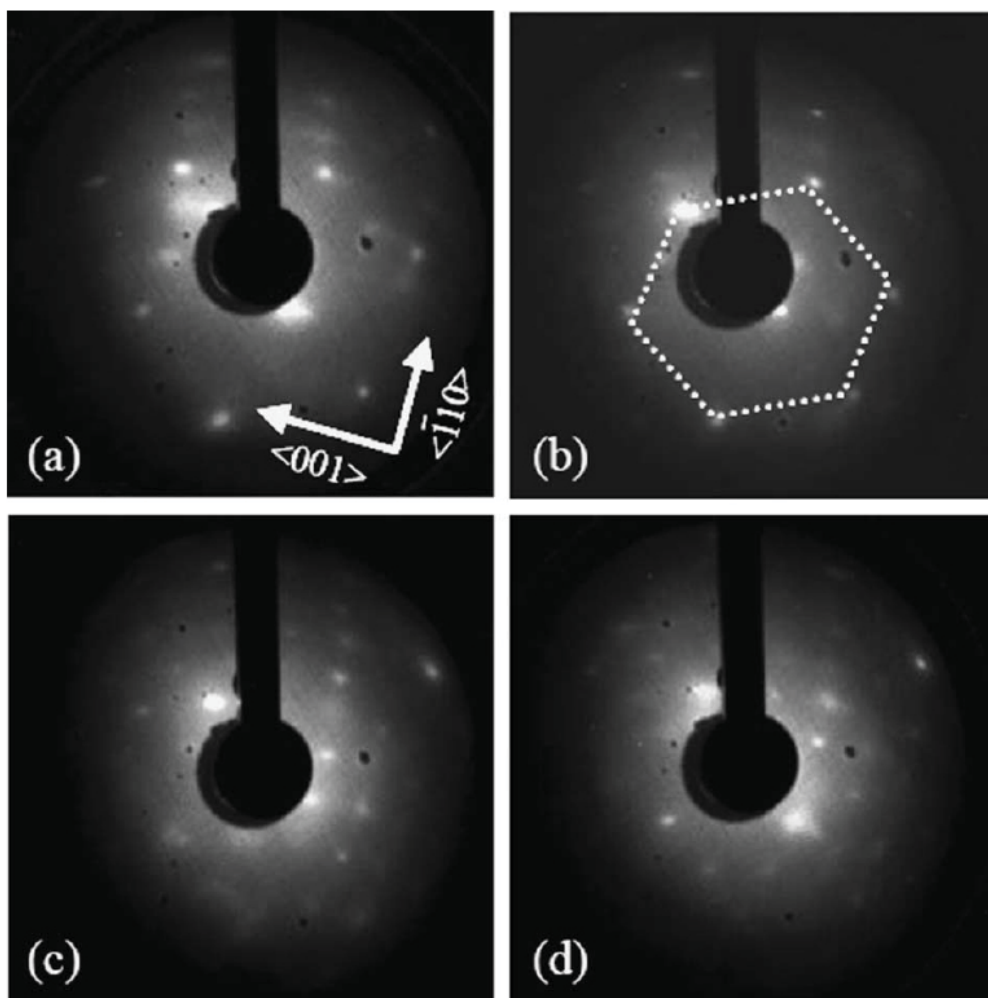


Figure 6. LEED patterns for the Co₃O₄(1 1 0)–Cu surface acquired at room temperature with incident electron beam energies at (a) 119 eV, (b) 128 eV, (c) 137 eV, and (d) 152 eV.

The $\text{Co}_3\text{O}_4(1\ 1\ 0)\text{-Cu}$ distorted hexagonal LEED pattern results from a copper-containing overlayer structure on top of the reduced spinel, since a weak rectangular diffraction pattern from the substrate can still be discerned in the LEED pattern but in poor quality and attenuated from the clean surface intensity. Several possibilities for the composition of this layer can be ruled out based on AES/XPS data and by comparison of the overlayer LEED pattern to the two-dimensional LEED patterns determined from kinematic calculations of other potential overlayer structures [48]. Surface structures considered include the impurity surface forming an incomplete Type B spinel termination layer [49], a mixed-metal copper cobalt oxide spinel layer [3, 11–14], a mixed-metal copper cobalt oxide solid solution [50], or a phase-separation copper oxide layer on the spinel surface [14, 27, 28]. The O/Co surface concentration ratio determined from AES and XPS data indicates a reduced surface, with insufficient oxygen to form a spinel as the majority species. Additionally, cobalt is now clearly in an octahedral Co^{2+} monoxide-like environment based on Co 2p spectral peak shapes. Therefore, only lower oxide compositions or phase-separated compounds need be considered.

While the formation of a mixed-metal monoxide $\text{Cu}_x\text{Co}_{1-x}\text{O}$ selvage or a phase-separated CuO/CoO -like overlayer could explain the stoichiometry of the $\text{Co}_3\text{O}_4(1\ 1\ 0)\text{-Cu}$ surface, neither copper-containing oxides form lattice planes with the symmetry and lattice spacing required by the LEED data. The $(1\ 1\ 0)$ plane of Cu_2O , however, reproduces the “distorted hexagonal” pattern overlayer structure very well. The packing structure of cuprite (Cu_2O) is body-centered cubic with respect to the oxygen atoms, and the 1+ copper cations occupy half the bridging sites between the center and the corner lattice sites of the cube (Fig. 7a). The bulk lattice parameter of Cu_2O is $a = 4.269\ \text{\AA}$ [51]. The $\text{Cu}_2\text{O}(1\ 1\ 0)$ plane has the correct symmetry to reproduce the LEED data and kinematic calculations of the two-dimensional LEED pattern show that it also has the correct lattice spacing. Kinematic LEED calculations were carried out using the available free-ware program SARCH from Van Hove [48].

The $\text{Cu}_2\text{O}(1\ 1\ 0)$ surface has two possible bulk termination layers, a copper layer and a copper and oxygen layer, labeled Type α and Type β in Fig. 7b and c. The copper layer (Type α) is a polar surface with lattice parameters of $2.610\ \text{\AA} \times 4.269\ \text{\AA}$ and, while kinematic LEED calculations yield a rect-

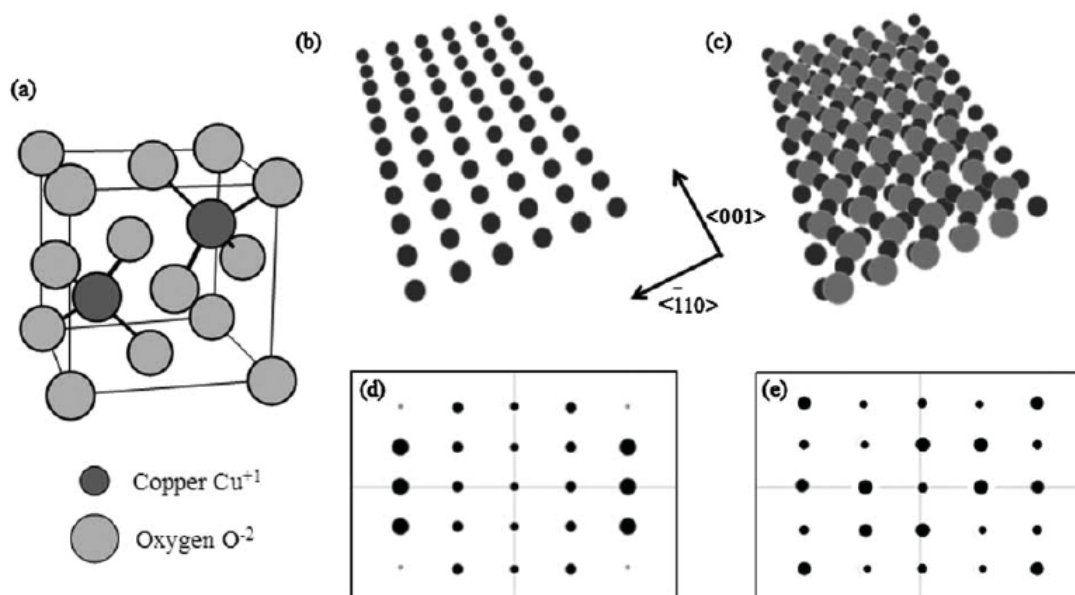


Figure 7. Cu_2O packing structure: (a) the unit cell and bulk lattice packing layers of the $(1\ 1\ 0)$ surface, (b) Type α polar Cu^{1+} layer, (c) Type β non-polar O–Cu zigzag layer, (d) the corresponding diffraction pattern for the Type α layer, and (e) the corresponding diffraction pattern for the Type β layer. Diffraction patterns were calculated kinematically.

angular pattern that might appear as a “distorted hexagon,” the copper–copper atomic lattice spacings do not match the experimental LEED overlayer lattice spacings. The Type β (1 1 0) termination layer, with both oxygen and copper ions, creates a more stable, non-polar surface shown in Fig. 7c. Based on bulk lattice parameters, the copper–copper lattice spacings of the Type β layer are $3.698 \text{ \AA} \times 4.269 \text{ \AA}$ along (0 0 1) and ($\bar{1}$ 1 0), respectively, and are within error of those of the distorted hexagonal LEED Cu-overlayer pattern ($3.86 \text{ \AA} \pm 0.2 \text{ \AA}$ along (0 0 1) and $4.10 \text{ \AA} \pm 0.2 \text{ \AA}$ along ($\bar{1}$ 1 0)). In the Type β (1 1 0) plane, the copper and oxygen atoms are arranged in a zigzag formation along the (0 0 1) direction.

The cobalt and copper AES integrated peak intensities were used to determine the surface Cu/Co saturation ratio of seven copper atoms per 10 cobalt atoms assuming the copper atoms were in an overlayer on top of the Co₃O₄ surface. However, a more realistic picture of the copper surface distribution can be obtained by more careful consideration of electron attenuation factors. The number of copper oxide overlayers, m , was calculated from the measured copper to cobalt AES integrated peak intensities through use of Eq. (1) [52]:

$$\frac{I_{\text{Cu}}}{I_{\text{Co}}} = \frac{\sum_{n=0}^m S_{\text{Cu}} C_{\text{Cu}} \exp\left(\frac{-nd_{\text{Cu}_2\text{O}}}{\lambda_{\text{Cu}_2\text{O}} \cos \theta}\right)}{\sum_{n=m+1}^{\infty} S_{\text{Co}} C_{\text{Co}} \exp\left(\frac{-xd_{\text{CoO}}}{\lambda_{\text{CoO}} \cos \theta}\right) \exp\left(\frac{-nd_{\text{Cu}_2\text{O}}}{\lambda_{\text{CoO}} \cos \theta}\right)} \quad (1)$$

In this equation, m is the Cu₂O overlayer thickness in monolayers and is the value determined from the calculation. I_{Cu} and I_{Co} are the AES integrated peak intensities, S_{Cu} and S_{Co} are the sensitivity factors taking in account the three Auger electron process, C_{Cu} and C_{Co} are the relative surface concentrations in atoms per cm², x is the number of CoO layers, $d_{\text{Cu}_2\text{O}}$ and d_{CoO} are the distance between the substrate layers of the specific lattice plane [51], $\lambda_{\text{Cu}_2\text{O}}$ and λ_{CoO} are the mean free paths of a Cu 2p and Co 2p electron passing through the sample to escape to the vacuum and be detected by the analyzer [51], $n = m + 1$ in the lower summation corrects for the number of Cu₂O overlayers covering the cobalt oxide substrate,

Table 1
Parameters used to calculate the Cu₂O overlayer thickness on the reduced Co₃O₄(1 1 0) spinel surface

Parameter	Value
$S_{\text{Cu}}/S_{\text{Co}}$	0.635 ^a
C_{Cu}	7.027×10^{13} atom/cm ²
C_{Co}	9.402×10^{13} atom/cm ²
$d_{\text{Cu}_2\text{O}}$	3.019 \AA (a)
d_{CoO}	3.008 \AA (a)
$\lambda_{\text{Cu}_2\text{O}}$	9.980 \AA (b)
λ_{CoO}	6.576 \AA (b)
θ	41° (c)

Letters in parentheses are from references: (a) [51], (b) [53] and (c) [54].

^a Value measured in-house experimentally using CuO and Cu₂O reference samples.

ues used in Eq. 1 are listed in Table 1. The number of monolayers of copper oxide on the cobalt oxide surface was determined from this calculation to be between 5 and 6 monolayers. The calculated copper oxide thickness assumes a complete and uniform coverage of the underlying cobalt oxide substrate, and does not consider the possibility of island formation. Island formation, if it occurs, would tend to increase the estimate of the copper oxide thickness depending upon the dispersion and island size.

The segregated copper overlayer was removed by flashing the sample to $\geq 700 \text{ K}$ (Fig. 4c). The resultant Auger spectrum of the spinel surface showed no copper Auger peaks to within the detection limit of the spectrometer. At this point, the substrate can then be easily re-oxidized back to the spinel stoichiometry, and the AES, XPS, and LEED data are again in agreement with those of the clean, stoichiometric Co₃O₄(1 1 0).

4. Discussion

Both stoichiometric and copper-segregated crystalline Co₃O₄(1 1 0) were characterized using the complementary surface sensitive techniques of AES, XPS, and LEED. The Co 2p XPS spectra for Co₃O₄(1 1 0) and Co₃O₄-Cu each had distinctive peak shapes and intensities that were used to distinguish between the stoichiometric spinel and the copper impurity-re-

duced substrate. The main cobalt $2p_{3/2}$ and $2p_{1/2}$ photoemission binding energies shifted upon copper segregation from 779.8 eV and 795.7 eV for the stoichiometric substrate to 779.2 eV and 795.2 eV for the copper-segregated surface, with substantial broadening to higher binding energy. The stoichiometric $\text{Co}_3\text{O}_4(1\ 1\ 0)$ surface showed the weak satellites expected for a diamagnetic Co^{3+} cation in an octahedral lattice site, with binding energies of 788.8 eV and 804.2 eV [32–35, 37, 38, 40, 41]. In contrast, the $\text{Co}_3\text{O}_4(1\ 1\ 0)\text{-Cu}$ surface showed intense satellite structure at 785.5 eV and 802.1 eV, characteristic of a CoO Co 2p XPS spectrum [19, 31–39]. The intense satellite peak structure for rocksalt monoxides results from strong final state effects in which the octahedrally coordinated Co^{2+} 3d levels hybridize with those of the O 2p lattice [39, 42]. These effects are not present in the spinel and the satellite structure and peak shapes can be used to distinguish between the two chemical environments for the cobalt [30, 32–34, 37].

From LEED data, the surface periodicity of the stoichiometric $\text{Co}_3\text{O}_4(1\ 1\ 0)$ surface was found to be $8.22\ \text{\AA} \pm 0.2\ \text{\AA}$ in the (0 0 1) direction and $5.50\ \text{\AA} \pm 0.2\ \text{\AA}$ in the $(\bar{1}\ 1\ 0)$ direction, in agreement with bulk spinel lattice parameters. The diffraction patterns (Fig. 2) are representative of the Type A bulk terminated (1 1 0) surface, with a rectangular symmetry and intensity variations based on the spinel packing structure in which both octahedral and tetrahedral lattice sites are partially occupied. The FCC packing of the oxygen lattice creates a (1/2, 1/2) subunit cell structure, which further modulated the diffraction spot intensities [49]. A net result is that the $\{1, 1\}$ and $\{\bar{1}, 1\}$ spots, and higher $2n$ diffraction multiples of these diffraction features, were generally observed to be more intense than other diffraction features (Fig. 2).

In comparison to the normal spinel structure of Co_3O_4 , magnetite (Fe_3O_4) crystallizes as an inverse spinel in which both the 2+ and 3+ cations equally occupy octahedral lattice sites and the remaining 3+ cations are found in the tetrahedral sites. From previously reported LEED [49] and STM [55] studies, it is known that $\text{Fe}_3\text{O}_4(1\ 1\ 0)$ undergoes a (3×1) surface reconstruction and does not terminate in ei-

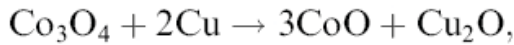
ther bulk termination lattice packing. This contrasts sharply with what is observed for the normal spinel $\text{Co}_3\text{O}_4(1\ 1\ 0)$ surface [30]. In order to preserve the general bulk structure in surface termination, the charges in the near surface region must be balanced so that any excess repulsive coulomb forces of the polar surface do not outweigh the increase in the surface tension that would result in going from a closer-packed, unreconstructed substrate to a more open, reconstructed substrate. For unreconstructed (1 1 0) termination, the spinel packing structure can result in either bulk layers, A or B, and while neither termination is charge neutral in the normal spinel, the unreconstructed inverse spinel surface has a greater charge imbalance for these two layers than does the regular spinel, which makes it more unstable. Therefore, the iron oxide surface has a greater driving force to reconstruct to eliminate the excess coulomb energy. Repulsive forces are insufficient to cause reconstruction in $\text{Co}_3\text{O}_4(1\ 1\ 0)$ and the surface retains its bulk termination structure.

The copper impurity-segregated $\text{Co}_3\text{O}_4(1\ 1\ 0)$ surface also was characterized by AES, XPS, and LEED. The Co 2p XPS data (Fig. 5) showed satellite structure characteristic of a CoO-like environment and the oxygen to cobalt atomic concentration decreased from 1.28 ± 0.15 for $\text{Co}_3\text{O}_4(1\ 1\ 0)$ to 0.94 ± 0.15 for $\text{Co}_3\text{O}_4(1\ 1\ 0)\text{-Cu}$, as calculated from the XPS peak intensities after correction for differences in O 1s and Co 2p cross sections [30]. The copper-segregated $\text{Co}_3\text{O}_4(1\ 1\ 0)\text{-Cu}$ phase separated to a 5–6 monolayer thick $\text{Cu}_2\text{O}(1\ 1\ 0)$ overlayer atop a reduced CoO-like near-surface selvage. The formation of the copper oxide layer occurred at the expense of the underlying Co_3O_4 substrate, creating an oxygen depleted layer to form copper oxide and reducing the cobalt oxide spinel to a cobalt monoxide-like surface. Further attempts to re-oxidize the reduced substrate were unsuccessful in transporting oxygen through the Cu_2O layer and thus pinned the $\text{Co}_3\text{O}_4(1\ 1\ 0)\text{-Cu}$ surface composition to that of the metal monoxide.

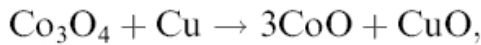
Since some substrate LEED intensity is found on even the most highly segregated copper oxide layers, this might suggest the possibility of island formation. The copper segregation appears to complete-

ly reduce the Co₃O₄(1 1 0) substrate to CoO-like in nature and, even if the underlying cobalt oxide substrate is not covered uniformly, the copper oxide must be fairly well-dispersed to affect the underlying substrate uniformly and to prevent re-oxidation to Co₃O₄. Small well-dispersed islands are entirely consistent with the poor, diffuse quality of the LEED pattern observe for the Cu₂O(1 1 0)-segregated surface. However, island formation is difficult to reconcile with the inability to re-oxidize the reduced cobalt oxide substrate unless all copper impurity is removed from the near-surface region. More information needs to be obtained to confirm or disprove island formation.

A possible reason for the surface reduction that accompanies copper segregation is that the copper impurity could be present as small copper inclusions formed during crystal growth. It is useful to consider the two solid state reactions:



$$\Delta_{\text{rxn}} G^0(298 \text{ K}) = -19.8 \text{ kJ}$$



$$\Delta_{\text{rxn}} G^0(298 \text{ K}) = +9.4 \text{ kJ}$$

Thermodynamic data [56] indicate that copper reduction of Co₃O₄ to form Cu₂O is favored at 298 K, whereas the formation of CoO is not. At the substrate pretreatment temperature used here, this effect becomes even more pronounced, with free energies of reaction estimated to be $\Delta_{\text{rxn}} G^0(630 \text{ K}) = -43.1 \text{ kJ}$ [56] for Cu₂O formation and $\Delta_{\text{rxn}} G^0(630 \text{ K}) = +2.7 \text{ kJ}$ for CuO formation. Because the reactions are solid state, the reactions are not explicitly dependent upon oxygen partial pressure and are only weakly dependent upon total pressure. Once formed as an overlayer atop the reduced cobalt oxide substrate, the Cu₂O might not permit sufficiently rapid oxygen transport to the reduced cobalt oxide for re-oxidation to Co₃O₄.

LEED symmetry and observed unit cell dimensions agree with the formation of Cu₂O(1 1 0). The Co₃O₄(1 1 0)-Cu LEED diffraction patterns revealed a distorted hexagonal structure attenuating the Type A Co₃O₄(1 1 0) diffraction pattern. Al-

though near hexagonal in symmetry, the LEED pattern for the Co₃O₄(1 1 0)-Cu surface showed measurably different unit cell spacings and is actually rectangular in symmetry. Relative to the underlying Type A Co₃O₄(1 1 0) lattice directions, the surface periodicity was measured to be $8.12 \text{ \AA} \pm 0.2 \text{ \AA}$ and $5.67 \text{ \AA} \pm 0.2 \text{ \AA}$ along the (0 0 1) and $(\bar{1} 1 0)$ directions, respectively. The “distorted hexagonal” unit cell is smaller than that of Co₃O₄(1 1 0) and the lattice spacings are not easily related to those of the substrate. Fig. 8 shows a potential arrangement for the Cu₂O(1 1 0) layer on the CoO-like reduced spinel. The Cu¹⁺ cations are assumed to be in tetrahedral lattice sites, while the O²⁻ anions are in FCC sites aligned along the (0 0 1) and $(\bar{1} 1 0)$ directions of the CoO(1 1 0)-like lattice. Even if the Cu₂O(1 1 0) is translated along the (0 0 1) and $(\bar{1} 1 0)$ directions to form different overlayer adsorption sites, the two substrates remain out of registry. It is clear from Fig. 8 that Cu₂O(1 1 0) forms an incommensurate overlayer.

As long as copper remained on the surface, the substrate was pinned to a metal monoxide concentration and could not be fully re-oxidized until the copper was eliminated. When the copper-segregated surface was heated to $\geq 700 \text{ K}$, copper was removed from the near surface region, most likely by desorption. Once the copper overlayer was removed by heating to $\geq 700 \text{ K}$, the near-surface region became depleted in the copper impurity and it became increasingly difficult to cause the copper to re-segregate by annealing at 630 K. Upon removal of the copper, the substrate was easily re-oxidized to the Co₃O₄ spinel stoichiometry by annealing under oxygen.

It is not uncommon for surface impurities to induce a surface reconstruction or to result in surface overlayer formation. For example, the inverse spinel Fe₃O₄(0 0 1) surface undergoes a surface reconstruction to a $p(1 \times 4)$ surface when Ca and K segregate to the surface after prolonged heating at 990 K [57, 58]. Similarly, when Fe₃O₄(0 0 1) thin films were grown on a MgO substrate, a $p(1 \times 4)$ surface reconstruction was observed to result from Mg²⁺ cations inter-diffusing throughout the iron oxide thin film [59, 60]. However, the Co₃O₄(1 1 0) surface is more energetical-

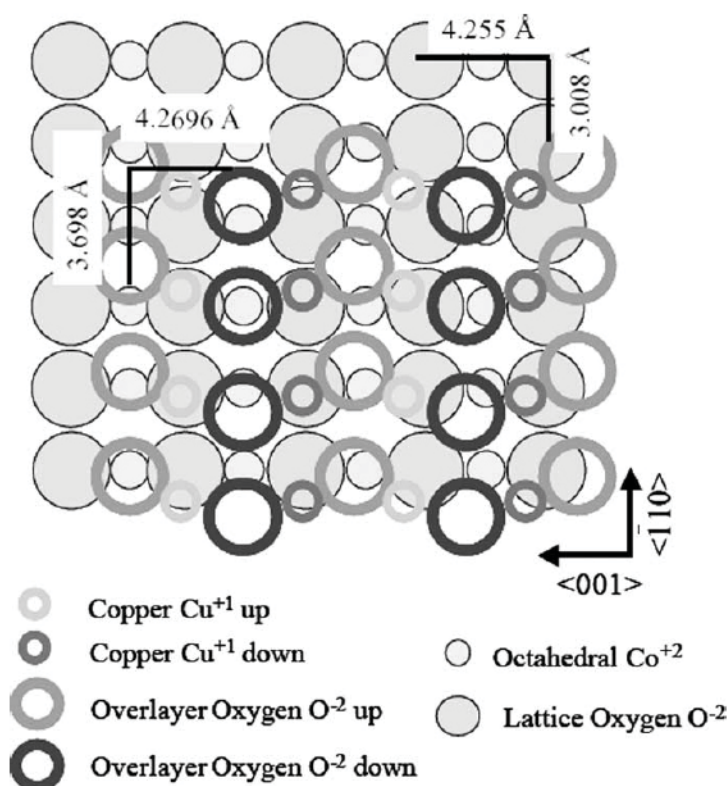


Figure 8. Possible atomic arrangement of the zigzag Type β $\text{Cu}_2\text{O}(1\ 1\ 0)$ overlayer on the CoO-like reduced $\text{Co}_3\text{O}_4(1\ 1\ 0)$ -Cu spinel surface. The two layers are incommensurate.

ly stable than the $\text{Fe}_3\text{O}_4(1\ 1\ 0)$ surface, which reconstructs with or without the presence of surface impurities, and the surface structure appears to be more robust. When alkali and alkaline earth surface impurities segregated to the $\text{Co}_3\text{O}_4(1\ 1\ 0)$ surface, they did not affect the surface structure in the present studies. This, in part, might be because they were only found at very low, submonolayer concentrations and the fate of the $\text{Co}_3\text{O}_4(1\ 1\ 0)$ structure at higher alkali and alkaline earth impurities is not known.

5. Conclusions

The $\text{Co}_3\text{O}_4(1\ 1\ 0)$ single crystal surface was successfully characterized using LEED, XPS, and AES. AES and XPS spectra were consistent with a stoichiometric Co_3O_4 spinel surface and LEED revealed a Type A spinel surface termination. The surface unit cell surface of the rectangular spinel lattice were measured as $8.22\ \text{\AA} \pm 0.2\ \text{\AA}$ and $5.50\ \text{\AA} \pm 0.2\ \text{\AA}$ in

the $(0\ 0\ 1)$ and $(\bar{1}\ 1\ 0)$ directions, respectively, which is within error of the bulk lattice parameters along these dimensions.

Upon extended annealing, Ca, K, Na, and Cu impurities segregated to the surface, and the copper impurity reduced the spinel selvage to a rocksalt metal monoxide-like surface stoichiometry. Copper impurity segregation was accompanied by changes in the LEED in which a distorted hexagonal overlayer diffraction pattern formed and attenuated that of the Type A rectangular spinel lattice. The new “distorted hexagon,” a rectangular surface structure with periodic spacing of $3.86\ \text{\AA} \pm 0.2\ \text{\AA}$ in the $(0\ 0\ 1)$ and $4.10\ \text{\AA} \pm 0.2\ \text{\AA}$ in the $(\bar{1}\ 1\ 0)$ directions, was consistent with the formation of $\text{Cu}_2\text{O}(1\ 1\ 0)$. The 5–6 monolayer thick $\text{Cu}_2\text{O}(1\ 1\ 0)$ overlayer formed at the expense of the near surface $\text{Co}_3\text{O}_4(1\ 1\ 0)$ substrate and reduced the cobalt oxide selvage to CoO-like in composition surface. The $\text{Co}_3\text{O}_4(1\ 1\ 0)$ substrate could not be fully re-oxidized until all detectable copper had been removed from the surface.

Acknowledgements

We gratefully acknowledge support from NSF under grant CHE-0213320, the Nebraska Research Initiative (NRI) and for the University of Nebraska Center for Materials Research and Analysis (CMRA).

References

- [1] J.P. Singh and R.N. Singh, *J. New Mater. Electrochem. Syst.* **3** (2000), p. 137.
- [2] N.-A.M. Deraz, *Mater. Lett.* **57** (2002), p. 914.
- [3] S. Angelov, G. Tyuliev and T. Marinova, *Appl. Surf. Sci.* **27** (1987), p. 381.
- [4] P. Thormahlen, M. Skoglundh, E. Fridell and B. Anderson, *J. Catal.* **188** (1999), p. 300.
- [5] R. Vijay, R.J. Hendershot, S.M. Rivera-Jimenez, W.B. Rogers, B.J. Feist, C.M. Snively and J. Lauterbach, *Catal. Commun.* **6** (2005), p. 167.
- [6] O.R. Van Buskirk, E.I. Du Pont of Nemours and Co., US Patent No. 4,310,596 (filed 1982).
- [7] W.M. Shaheen and A.A. Ali, *Mater. Res. Bull.* **36** (2001), p. 1703.
- [8] J. Jansson, *J. Catal.* **194** (2000), p. 55.
- [9] B.A. Sexton, A.E. Hughes and T.W. Turney, *J. Catal.* **97** (1986), p. 390.
- [10] V.E. Henrich and P.A. Cox, *The Surface Science of Metal Oxides*, Cambridge University Press, Cambridge (1994).
- [11] S. Angelov, D. Mehandjiev, B. Piperov, V. Zarkov, A. Terlecki-Baricevic, D. Jovanovic and Z. Jovanovic, *Appl. Catal.* **16** (1985), p. 431.
- [12] K. Krezhov, K. Petrov and T. Karamaneva, *J. Solid State Chem.* **48** (1983), p. 33.
- [13] I. Rasines, *J. Appl. Crystallogr.* **5** (1972), p. 11.
- [14] S. Angelov, E. Zhecheva, K. Petrov and D. Mehandjiev, *Mater. Res. Bull.* **17** (1982), p. 235.
- [15] K.J. Kim, Y.R. Park, D.H. Hyun and S.H. Lee, *J. Appl. Phys.* **96** (2004), p. 1975.
- [16] D. Pyke, K.J. Mallick, R. Reynolds and A.K. Bhattacharya, *J. Mater. Chem.* **8** (1998), p. 1095.
- [17] Nikolov, R. Darkaoui, E. Zhecheva, R. Stoyanova, N. Dimitrov and T. Vitanov, *J. Electroanal. Chem.* **429** (1997), p. 157.
- [18] J.L. Gautier, R. Rios, M. Garcia, J.F. Marco and J.R. Gancedo, *Thin Solid Films* **311** (1997), p. 51.
- [19] J.G. Kim, D.L. Pugmire, D. Battaglia and M.A. Langell, *Appl. Surf. Sci.* **165** (2000), p. 70.
- [20] B. Marcus-Saubat, J.P. Beaufile and Y. Barbaux, *J. Chim. Phys. Phys.—Chim. Biol.* **83** (1986), p. 317.
- [21] J.L. Hutchinson and N.A. Briscoe, *Ultramicroscopy* **18** (1985), p. 435.
- [22] W.L. Smith, *Acta Cryst.* **329** (1973), p. 362.
- [23] W.L. Roth, *J. Phys. Chem. Solids* **25** (1964), p. 1.
- [24] B. Pejova, A. Isahi, M. Najodski and I. Grozdanov, *Mater. Res. Bull.* **36** (2001), p. 161.
- [25] P.A. Cox, *Transition Metal Oxides: An Introduction to their Electronic Structure and Properties*, Clarendon Press, Oxford (1992).
- [26] S.A. Chambers In: D.P. Woodruff, Editor, *The Chemical Physics of Solid Surfaces* vol. **6**, Elsevier Science: North Holland (2001), p. 301.
- [27] T.M. Tsai, K.C. Yang and P. Shen, *J. Solid State Chem.* **177** (2004), p. 3301.
- [28] G. Fierro, M. Lo Jacono, M. Inversi, R. Dragone and P. Porta, *Top. Catal.* **10** (2000), p. 39.
- [29] K.M.E. Miedzinska, R.B. Hollebone and J.G. Cook, *Can J. Phys. Chem. Solids* **48** (1987), p. 649.
- [30] S.C. Petitto and M.A. Langell, *J. Vac. Sci. Technol. A* **22** (2004), p. 1690.
- [31] E.M. Malone, S.C. Petitto and M.A. Langell, *Solid State Commun.* **130** (2004), p. 571.
- [32] G.A. Carson, M.H. Nassir and M.A. Langell, *J. Vac. Sci. Technol. A* **14** (1996), p. 1637.
- [33] M.A. Langell, G.A. Carson, S. Smith, L. Peng and M.H. Nassir, *Mater. Res. Soc. Sympos. Proc.* **547** (1999), p. 255.
- [34] G.A. Carson, M.H. Nassir and M.A. Langell, *Surf. Sci. Spectra* **5** (1998), p. 235.
- [35] T.J. Chuang, C.R. Brundle and D.W. Rice, *Surf. Sci.* **59** (1976), p. 413.
- [36] V.M. Jimenez, A. Fernandez, J.P. Espinos and A.R. Gonzales-Elipe, *J. Electron Spectrosc. Relat. Phenom.* **71** (1995), p. 61.
- [37] J. van Elp, J.L. Wieland, H. Eskes, P. Kuiper, G.A. Sawatsky, R.M.F. de Groot and T.S. Turner, *Phys. Rev. B* **44** (1991), p. 6090.
- [38] N.S. McIntyre and M.G. Cook, *Anal. Chem.* **47** (1975), p. 2208.
- [39] Z.X. Shen, J.W. Allen, P.A.P. Lindberg, D.S. Dessau, B.O. Wells, A. Borg, W. Ellis, J.S. Kang, S.J. Oh, I. Lindau and W.E. Spicer, *Phys. Rev. B* **42** (1990), p. 1817.
- [40] M. Oku and Y. Sato, *Appl. Surf. Sci.* **55** (1992), p. 37.
- [41] M.A. Langell, C.W. Hutchings, G.A. Carson and M.H. Nassir, *J. Vac. Sci. Technol. A* **14** (1996), p. 1656.
- [42] L.C. Davis, *Phys. Rev. B* **25** (1982), p. 2912.
- [43] M.A. Langell, G.A. Carson, M. Anderson, L. Peng and S. Smith, *Phys. Rev. B* **59** (1999), p. 4791.
- [44] S. Angelov, E. Zhecheva, R. Stoyanova and M. Atanasov, *Phys. Chem. Solids* **51** (1990), p. 1157.
- [45] L.J. Clarke, *Surface Crystallography: An Introduction to*

- Low Energy Electron Diffraction, John Wiley & Sons, New York (1985).
- [46] R.W.M. Kwok. Available from:
<http://www.phy.cuhk.edu.hk/~surface/XPSPEAK>
- [47] D.A. Shirley, *Phys. Rev. B* **5** (1972), p. 4709.
- [48] M.A. Van Hove, SARCH = Surface Architect + Latuse + Plot3D_Version 4.01, 1995. Available from:
<http://w3.rz-berlin.mpg.de/~hermann/SLP/>
- [49] Y. Oda, S. Mizuno, S. Todo, E. Torikai and K. Hayakawa, *Jpn. J. Appl. Phys.* **37** (1998), p. 4518.
- [50] L.A. Zabdyr and O.B. Farichnaya, *J. Phase Equilib.* **23** (2002), p. 149.
- [51] R.W.G. Wyckoff, *Crystal Structures*, Interscience Publishers, New York (1963).
- [52] D. Briggs and M.P. Seah, *Practical Surface Analysis*, Wiley, New York (1990).
- [53] D.R. Penn, *J. Electron Spectrosc. Relat. Phenom.* **9** (1976), p. 29.
- [54] M.A. Langell, C.L. Berrie, M.H. Nassir and K.W. Wulser, *Surf. Sci.* **320** (1994), p. 25.
- [55] R. Jansen, V.A.M. Brabers and H. van Kempen, *Surf. Sci.* **328** (1995), p. 237.
- [56] Thermodynamic data obtained from the NIST Webbook. Available from:
<http://webbook.nist.gov/chemistry/form-ser.html.en-us.en>
- [57] G. Mariotto, S. Murphy, N. Berdunov, S.F. Ceballos and I.V. Shvets, *Surf. Sci.* **564** (2004), p. 79.
- [58] A.P. Sutton and R.W. Balluffi, *Interfaces in Crystalline Materials*, Oxford University, Oxford (1996).
- [59] J.F. Anderson, M. Kuhn, U. Diebold, K.A. Shaw, P. Stoyanov and D.M. Lind, *Phys. Rev. B* **56** (1997), p. 9902.
- [60] K.A. Shaw, E. Lochner and D.M. Lind, *J. Appl. Phys.* **87** (2000), p. 1727.